A Hybrid Diagnosis Method for Inverter Open-circuit Faults in PMSM Drives

Zeliang Zhang, Guangzhao Luo, *Senior Member, IEEE,* Zhengbin Zhang, and Xuecheng Tao

***Abstract*—In order to improve the evaluation process of inverter open-circuit faults diagnosis in permanent magnet synchronous motor (PMSM) drives, this paper presents a diagnosis method based on current residuals and machine learning models. The machine learning models are introduced to make a comprehensive evaluation for the current residuals obtained from a state observer, instead of evaluating the residuals by comparing with thresholds. Meanwhile, fault diagnosis and location are conducted simultaneously by the machine learning models, which simplifies the diagnosis process. Besides, a sampling strategy is designed to implement the proposed scheme online. Experiments are carried out on a DSP based PMSM drive，and the effectiveness of the proposed method is verified.**

***Index Terms*—Current residuals, fault diagnosis, inverter open-circuit, machine learning.**

I. INTRODUCTION

IN Permanent-Magnet Synchronous Motor(PMSM) drives, inverters are the closest link between digital control and power output, and also the weak link where faults are diverse and occur frequently. According to statistics, about 38% of the faults in motor drives are due to failures of inverters [1]. Inverter faults can be classified into short-circuit and open-circuit. Short-circuit faults will lead to immediate over-current. Therefore, protective circuits are required for quick response, or short-circuit can be converted to open-circuit by thermo-fuse [2]. Conversely, open-circuit will not cause an immediate shutdown, but the current imbalance and torque ripple caused by faults will lead to secondary damage [3].

Generally, diagnosis methods for inverter open-circuit can be categorized as signal analysis method, model-based method, and data-driven method. Among them, signal analysis method was the first broadly applied method [4] [5] [6]. Reference [7] proposes a diagnosis method based on the ratio between line voltages. Line voltage deviations and phase voltage deviations are combined to classify open-circuit faults and current sensor faults in [8]. Reference [9] performs diagnosis by monitoring the residence time of the park's vector in each sector of the $\alpha\beta$ coordinate. Reference [10] carries out a comparative study of four current-vector based methods. Signal analysis is easy to implement, but as control strategies become more and more complex, the fault information hidden in the signals has also become increasingly difficult to extract and summarize.

Aiming at obtaining more informative diagnosis variables, model-based method emerged [11]. In [12] [13], the three-phase current is estimated using Luenburger observer, and an adaptive threshold is designed to evaluate residuals. Based on mixed-logic-dynamic model, References [14] [15] construct current observer and voltage observer respectively, to obtain residuals. Reference [16] employs model reference adaptive system to estimate the distortion of phase voltages, and diagnostic decisions are made by comparing voltage distortion with a threshold. In [17], a sliding mode observer is employed to estimate currents, and the faults are also diagnosed by comparing the current residuals with thresholds. In the model-based method, observation residuals are immune to the changes in load and speed, however, evaluating the residuals by comparing with a threshold are unable to classify the fault patterns whose responses show similarity, which results in underutilization of the information in the diagnosis variables.

For the purpose of comprehensively evaluating the diagnosis variables, data-driven method was introduced. In [18], normalized current-vector is introduced as diagnosis variable, and the diagnosis results are determined by fuzzy inference. In [19], a training set consisting of the phase voltage, phase current, and torque is used to train a neural network. In [20], the discrete-time wavelet transform is performed to extract the features of the phase currents, and then the faulty patterns are recognized by support vector machine (SVM). In [21], signal features of line voltages are extracted by FFT, and the fault diagnosis is performed using a Bayesian network. Data-driven method studies the distribution features of the training set to fully utilize the diagnostic information in the samples. However, the quality of the samples of the diagnosis variables has a decisive influence on the results. Meanwhile, data-driven method is difficult to implement online.

This paper proposes a hybrid diagnosis scheme in which the machine learning models are introduced to fully evaluate and utilize the fault information contained in the current residuals. Besides, a sampling strategy is presented to achieve online implementation. As depicted in Fig. 1: A observer is introduced to obtain current residuals as diagnosis variables; then, the residual samples are collected using the designed sampling strategy; after that, the machine learning models are trained

Manuscript was submitted for review on 07, April, 2020.

Zeliang Zhang, Guangzhao Luo, Xuecheng Tao are with the School of Automation, Northwestern Polytechnical University, Xi'an 710129, China (e-mail:18829237032@163.com,guangzhao.luo@nwpu.edu.cn,1165735220@qq.com). (Corresponding author: Prof. Guangzhao Luo).

Zhengbin Zhang is with Lanzhou Wanli Aviation Electromechanical Co.Ltd, Lanzhou 730070, China (e-mail: binbincool.ok@163.com).

Digital Object Identifier 10.30941/CESTEMS.2020.00023

offline based on the samples; finally, the samples of different fault patterns are classified by the machine learning models online. The proposed diagnosis method is integrated into the control cycles and does not cause any influence on the motor control. The experimental results show that the proposed method can locate faults in less than half a fundamental period. The rest of this paper is organized as follows: In Section II, the effects of open-circuit on PMSM drive are analyzed. Section III introduces the proposed hybrid diagnosis method. Finally, the simulation and experimental results are presented in Section IV and Section V respectively.

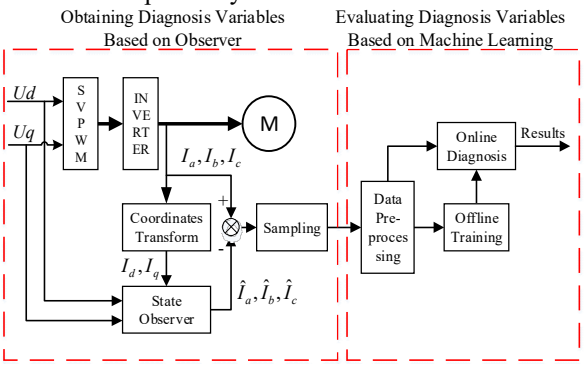

Fig. 1. Block diagram of the proposed diagnosis method.

II. Influence of Inverter Open Circuit

The inverter in PMSM drive is shown in Fig. 2. When no faults occur, the inverter has six inherent space voltage vectors and two zero vectors. When open-circuit occurs, the faulty devices are no longer controlled by the PWM signals, resulting in changes on the inherent vectors. Also, the magnitudes and directions of the synthesized vectors that control the motion of the stator flux are changed. This section takes T1 open-circuit as an example to study the impacts of open-circuit on voltage vectors and stator flux and analyzes the system responses.

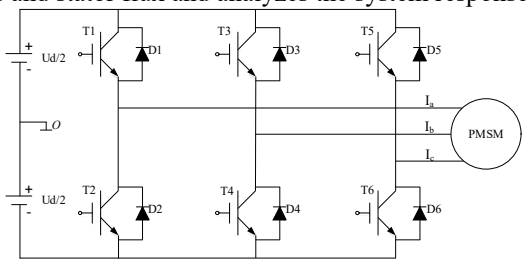

Fig. 2. Three-phase inverter topology.

A. The Influence on Space Voltage Vectors and Stator Flux

The inherent space vectors and their corresponding three-phase PWM signals are shown in Fig. 3, where "1" indicates that the driving signal for the upper arm is "High", and "0" indicates that the driving signal for the lower arm is "High".

As can be seen from Fig. 3, T1 open-circuit will affect the inherent vectors $\overrightarrow{u_4}$, $\overrightarrow{u_5}$ and $\overrightarrow{u_6}$. For $\overrightarrow{u_4}$, since the current path connected to the positive pole of the DC source is blocked, there is no circuit paths in the inverter, resulting in $\overrightarrow{u_4}$ turning into a zero vector. For $\overrightarrow{u_5}$ and $\overrightarrow{u_6}$, T1 open-circuit also blocks the positive current path flowing through the phase-A leg, but there are still current paths flowing through the other two legs. So, T1 open-circuit causes changes on the magnitudes and spatial directions of these two space vectors and turns them into $\overrightarrow{u_5^f}$ and $\overrightarrow{u_6^f}$. The impacts on $\overrightarrow{u_5}$ and $\overrightarrow{u_6}$ are shown in Fig. 4:

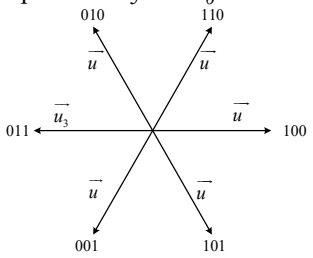

Fig. 3. Six inherent space voltage vectors.

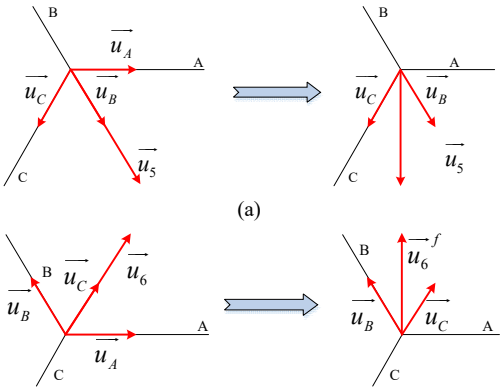

Fig. 4. The influence of T1 open circuit on $\overrightarrow{u_5}$. (b) The influence of T1 open circuit on $\overrightarrow{u_6}$.

Therefore, when T1 open-circuit occurs, the inverter has five inherent space voltage vectors, as shown in Fig. 5:

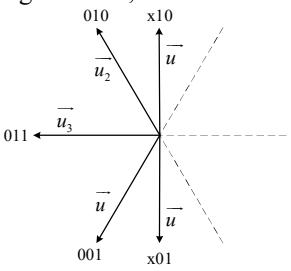

Fig. 5. Inherent space voltage vectors after T1 open circuit.

In FOC, $\overrightarrow{u_i}$ is orthogonal to the stator flux $\overrightarrow{\Psi_s}$, and determines the direction and magnitude of the increment of $\overrightarrow{\Psi_s}$, which represents as $\Delta\overrightarrow{\Psi_s}$. The magnitude of $\Delta\overrightarrow{\Psi_s}$ depends on the acting time of each $\overrightarrow{u_i}$, that is, $\Delta\overrightarrow{\Psi_s}=\overrightarrow{u_i}\times\Delta t$. In SVPWM, $\overrightarrow{\Psi_s}$ is controlled to move in a round trace by alternating action of two adjacent inherent vectors and zero vectors in each switching period. When controlling $\overrightarrow{\Psi_s}$ to rotate counterclockwise, the two space vectors corresponding to each spatial sector before and after the fault occurs are shown in Fig. 6:

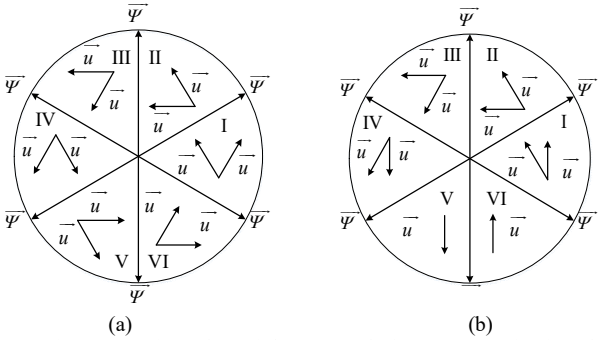

Fig. 6. Acting vectors in each spatial sector. (a)before T1 open circuit and (b)after T1 open circuit.

It is known from Fig. 6 and Fig. 5 that the vectors acting at sector I, IV, V, and VI change after T1 open-circuit. Suppose the synthesized vector is $\overrightarrow{u_s}$, the acting time of two adjacent space vectors and zero vectors in each sector is t_1, t_2, and t_3. Then the changes of $\overrightarrow{u_s}$ in each sector are shown in Table I:

TABLE I
THE INFLUENCE OF T1 OPEN CIRCUIT ON SYNTHESIZED VECTOR

Sectors	Synthesized vector before fault occurs	Synthesized vector after fault occurs
I	$\overrightarrow{u_s}=t_1\overrightarrow{u_6}+t_2\overrightarrow{u_2}+t_3(\overrightarrow{u_0}+\overrightarrow{u_7})$	$\overrightarrow{u_s}=t_1\overrightarrow{u_6}^f+t_2\overrightarrow{u_2}+t_3(\overrightarrow{u_0}+\overrightarrow{u_7})$
II	$\overrightarrow{u_s}=t_1\overrightarrow{u_2}+t_2\overrightarrow{u_3}+t_3(\overrightarrow{u_0}+\overrightarrow{u_7})$	No changes
III	$\overrightarrow{u_s}=t_1\overrightarrow{u_3}+t_2\overrightarrow{u_1}+t_3(\overrightarrow{u_0}+\overrightarrow{u_7})$	No changes
IV	$\overrightarrow{u_s}=t_1\overrightarrow{u_1}+t_2\overrightarrow{u_5}+t_3(\overrightarrow{u_0}+\overrightarrow{u_7})$	$\overrightarrow{u_s}=t_1\overrightarrow{u_1}+t_2\overrightarrow{u_5}^f+t_3(\overrightarrow{u_0}+\overrightarrow{u_7})$
V	$\overrightarrow{u_s}=t_1\overrightarrow{u_5}+t_2\overrightarrow{u_4}+t_3(\overrightarrow{u_0}+\overrightarrow{u_7})$	$\overrightarrow{u_s}=t_1\overrightarrow{u_5}^f+t_3(\overrightarrow{u_0}+\overrightarrow{u_4}+\overrightarrow{u_7})$
VI	$\overrightarrow{u_s}=t_1\overrightarrow{u_4}+t_2\overrightarrow{u_6}+t_3(\overrightarrow{u_0}+\overrightarrow{u_7})$	$\overrightarrow{u_s}=t_1\overrightarrow{u_6}^f+t_3(\overrightarrow{u_0}+\overrightarrow{u_4}+\overrightarrow{u_7})$

The magnitudes of $\overrightarrow{u_5}$ and $\overrightarrow{u_6}$ are reduced to $\sqrt{3}/2$ of the original, and the acting time of $\overrightarrow{u_4}$ is allocated to zero vectors. These effects reduce the magnitude of $\Delta\overrightarrow{\Psi_s}$ and change the trace of $\overrightarrow{\Psi_s}$, resulting in decreases in motor speed and torque

B. System responses of PMSM drive under T1 open-circuit

From the analysis in the previous part, it is known that the reasons for the drops on motor speed and torque are that the magnitudes of the voltage vectors are reduced, and the acting time of zero vectors is increased. However, with the drop of motor speed, the duty cycle of PWM signals will rise due to the closed-loop regulation, so that the acting time of non-zero vectors will increase, leading to the motor speed rebound, and finally the speed fluctuation will occur.

The T1 open-circuit is simulated on an inverter fed PMSM. The speed command is 1500 rpm, with a constant load of 5 N.m, and the simulation time is 1s. At 0.5s, T1 open-circuit is simulated by blocking the driving signal of T1. The three-phase current regulation and speed fluctuation caused by T1 open circuit are shown in Fig. 7:

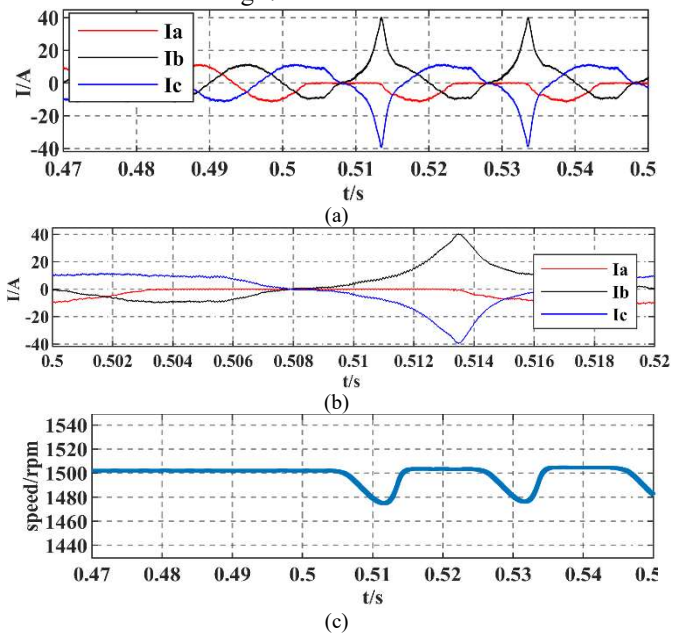

Fig. 7. Three-phase current under T1 open circuit, Three-phase current under T1 open circuit from 0.5 s to 0.52 s :(c) Speed response under T1 open circuit.

In simulation, T1 open-circuit occurs at 0.5 s when $\overrightarrow{\Psi_s}$ is moving in sector III (acting vectors are $\overrightarrow{u_1}$ and $\overrightarrow{u_3}$) where $I_c > 0 > I_b > I_a$. At about 0.502 s, $\overrightarrow{\Psi_s}$ moves to the upper half of sector IV (acting vectors are $\overrightarrow{u_1}$ and $\overrightarrow{u_5}^f$), where $I_c > 0 > I_a > I_b$. Starting from around 0.503 s, $\overrightarrow{\Psi_s}$ rotates in the lower half of sector IV and sector V (acting vector is $\overrightarrow{u_5}^f$), and at about 0.508 s, $\overrightarrow{\Psi_s}$ moves to sector VI (acting vector is $\overrightarrow{u_6}^f$). When $\overrightarrow{\Psi_s}$ rotates in sector V and sector VI, motor speed drops due to the decrease in the magnitudes of the non-zero vectors and the increase in the acting time of zero vectors. Until around 0.512 s, $\overrightarrow{\Psi_s}$ moves to the upper half of sector I (acting vectors are $\overrightarrow{u_2}$ and $\overrightarrow{u_6}^f$). At this time, due to the closed-loop regulation, the acting time of non-zero vectors increases and motor speed starts to rise.

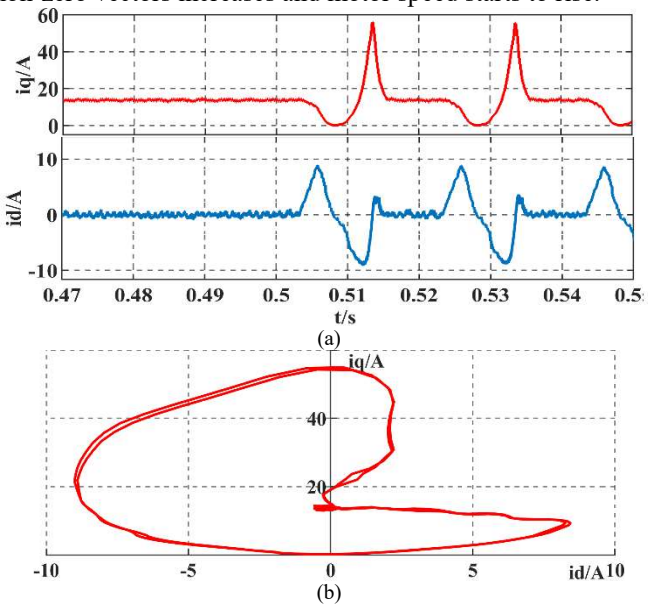

Fig. 8.(a) i_q and i_d under T1 open circuit, (b) The trace of the magnitude of the current vector in *dq* coordinate.

At about 0.508s, the magnitude of the current-vector in *dq* coordinate is zero, which represents the electromagnetic torque is zero. This is because $\overrightarrow{\Psi_s}$ moves to the junction of sector V and sector VI at this moment, and $\overrightarrow{u_4}$ orthogonal to $\overrightarrow{\Psi_s}$ here turns into a zero vector, making the inverter unable to supply power to the motor. It can be seen from Fig. 8 that the trace of the current vector varies in a large range around the q-axis, and a large part of the current vector acts on d-axis, which generates reactive power. Thus, even if the speed does not continuously drop but fluctuates around the speed command under the regulation of the controller, the efficiency of PMSM drive declines severely.

Inverter open-circuit will cause changes in the responses and state variables. But the system feedbacks and state variables are susceptible to changes in motor load and speed, and applying these changes directly for diagnosis can easily lead to misdiagnosis. Hence, before making evaluation and decisions, obtaining qualified diagnosis variables is essential.

III. THE HYBRID DIAGNOSIS METHOD BASED ON CURRENT RESIDUALS AND MACHINE LEARNING MODELS

A. Diagnosis variables based on Luenburger observer

The qualified diagnosis variables should have the following characteristics, which are a) When the system operating with no faults, the diagnosis variables should remain constant even the operating condition changes, and b) When faults occur, the variables can deviate from the constant point rapidly and show different features according to different fault patterns.

A Luenburger observer is introduced to obtain current residuals as the diagnosis variables. Firstly, when the inverter is healthy, the observer can quickly track i_d and i_q, regardless of changes in the load and speed, to meet the first characteristic. Secondly, due to the sudden changes of currents while faults occur, the feedback gains of the observer are unable to make the residuals converge rapidly, so the residuals deviate from zero which meet the second characteristic.

i_d and i_q are estimated, and then the estimated three-phase current are obtained through inverse coordinate transformation. The dynamic model of PMSM is shown below:

$$\begin{pmatrix} \frac{di_d}{dt} \\ \frac{di_q}{dt} \end{pmatrix} = \begin{pmatrix} -\frac{R_s}{L} & \omega_e \\ -\omega_e & -\frac{R_s}{L} \end{pmatrix} \begin{pmatrix} i_d \\ i_q \end{pmatrix} + \begin{pmatrix} \frac{1}{L} & 0 \\ 0 & \frac{1}{L} \end{pmatrix} \begin{pmatrix} u_d \\ u_q \end{pmatrix} + \begin{pmatrix} 0 \\ -\frac{\omega_e \psi_f}{L} \end{pmatrix} \quad (1)$$

where i_d, i_q, u_d, u_q, and L are currents, voltages, and inductance on dq-axes; R_s is the stator resistance; ω_e is the electrical angular velocity and ψ_f indicates the rotor flux linkage.

Transform the dynamic model into the general form of the linear system as below:

$$\begin{cases} \dot{x}(t) = Ax(t) + Bu(t) + D \\ y(t) = Cx(t) \end{cases} \quad (2)$$

where

$$x(t) = \begin{pmatrix} i_d \\ i_q \end{pmatrix} \quad u(t) = \begin{pmatrix} u_d \\ u_q \end{pmatrix} \quad C = \begin{pmatrix} 1 & 0 \\ 0 & 1 \end{pmatrix} \quad (3)$$

The observability matrix of this linear system is shown as:

$$O = [C \; CA \; ... \; CA^{n-1}]^T = \begin{pmatrix} 1 & 0 & -\frac{R_s}{L} & \omega_e \\ 0 & 1 & -\omega_e & -\frac{R_s}{L} \end{pmatrix} \quad (4)$$

It can be seen that O is a nonsingular matrix. Therefore, the state observer can be constructed to observe i_d and i_q as shown below, and then the three-phase current can be reconstructed through inverse coordinate transformation.

$$\begin{cases} \dot{\hat{x}}(t) = A\hat{x}(t) + Bu(t) + D + K(y(t) - \hat{y}(t)) \\ \hat{y}(t) = C\hat{x}(t) \end{cases} \quad (5)$$

where $\hat{x}(t)$ and $\hat{y}(t)$ are the estimated values of $x(t)$ and $y(t)$; K is the feedback gain matrix which represents as:

$$K = \begin{pmatrix} K_1 & 0 \\ 0 & K_2 \end{pmatrix} \quad (6)$$

The feedback gains determine the dynamic performance of the observer. Assume the error between the observed value and the feedback is e:

$$\begin{cases} e = x - \hat{x} \\ \dot{e} = \dot{x} - \dot{\hat{x}} \end{cases} \quad (7)$$

Substituting equation (2) and (5) into (7) gives:

$$\dot{e} = (A - KC)e \quad (8)$$

Equation 8 is a homogeneous differential equation, which can be solved as:

$$e(t) = \exp((A - KC)t)e(t_0), \quad t \geq 0 \quad (9)$$

It can be seen that when the eigenvalues of $(A - KC)$ have negative real parts, e has asymptotic stability. The larger the absolute values of the negative real parts are, the faster the error e converges. In this paper, by configuring the feedback gains, e can either converge when the inverter is healthy or deviate from zero when current feedbacks are lost.

B. The evaluation process based on PCA and SVM

Indeed, the observer can provide stable and informative diagnosis variables. However, because different open-circuit faults share same conduction paths in the inverter, the responses of the observer under different open-circuit faults show similarity. In these cases, it is difficult to distinguish these faults by comparing with thresholds.

The main defect of comparing residuals with thresholds is that only the magnitude relationship is concerned, but the dynamic feature of current residuals in a range of phase is neglected. Another defect is that the magnitude relationship is inducted empirically, which generally leads to excessive margins to avoid false trigger but degrades the sensitivity.

Different from comparing with thresholds, machine learning models evaluate residuals by extracting and classifying the distribution features of the samples in a range of phase. These features are not extracted empirically, but have statistical significance. Also, the machine learning models simplify the diagnosis process by simultaneously diagnosing and locating the faults.

Compared with the typical tasks of machine learning, such as text recognition, diagnosis of inverter open-circuit is a small sample case. First of all, the quantity of sample patterns is small. There are 21 types of single IGBT open-circuit and double IGBTs open-circuit, which are far less than the sample patterns of text recognition. Secondly, the sample dimension is small. Taking the system sampling frequency of 10 kHz and sampling the three-phase current residual in half an electrical cycle, the dimension of each sample varies from tens to hundreds depending on different sampling rates. Therefore, machine learning models for diagnosis of inverter open circuit faults should be suitable for small sample task. In this paper, diagnosis variables are evaluated using Principal Component Analysis (PCA) and Support Vector Machine (SVM) due to their suitability for small sample task.

Set N samples as $\{(\vec{x_i}, y_i)\}_{i=1}^{N}$, where $\vec{x_i}$ is a sample vector, y_i is the label of $\vec{x_i}$ and $y_i \in [-1,1]$. The basic problem of machine learning is to find a classification hyperplane, expressed as $\vec{\omega}^T\vec{x}+b$, where $\vec{\omega}$ is the coefficient vector, $\vec{x}$ is the sample vector, and b is a coefficient. SVM first finds support vectors closest to the hyperplane. The margins between the support vectors and the hyperplane are expressed as:

$$margin(\vec{\omega}, \vec{x}_i, b) = \min_{\vec{\omega}, \vec{x}_i, b} \frac{1}{\|\vec{\omega}\|} \left| \vec{\omega}^T \vec{x}_i + b \right| \quad (10)$$

According to the maximal margin principle, the optimization

objective and constraints of SVM are as follows:

$$\begin{cases} \max\limits_{\vec{\omega},b} \min\limits_{\vec{x}_i} \dfrac{1}{\|\vec{\omega}\|} \left| \vec{\omega}^T \vec{x}_i + b \right| \\ s.t. \ \begin{cases} \vec{\omega}^T \vec{x}_i + b > 0, y_i = 1 \\ \vec{\omega}^T \vec{x}_i + b < 0, y_i = -1 \end{cases} \end{cases} \tag{11}$$

Simplifying the optimization objective and combining the constraints. The optimization problem is transformed into a standard quadratic programming problem with N constraints to solve $\vec{\omega}$ and b:

$$\begin{cases} \min\limits_{\vec{\omega},b} \dfrac{1}{2} \vec{\omega}^T \vec{\omega} \\ s.t. \ y_i(\vec{\omega}^T \vec{x}_i + b) \ge 1, i = 1, ..., N \end{cases} \tag{12}$$

$\vec{\omega}$ and b are solved by finding the extremum under the constraints of the samples, instead of based on the maximum likelihood estimation. Therefore, SVM is independent of the probability density of the samples. The goal is to obtain the optimal solution under limited samples, not only when the number of samples tends infinity. Hence, SVM is suitable for the case of limited and small samples.

PCA does not involve the probability density of samples as well but is based on the variances and covariances of the projections of samples. PCA looks for a new coordinate system so that a few coordinates of the samples in the new coordinate system can represent most of the information. The dimension reduction model is a set of the unit vectors of an orthogonal coordinate system. Suppose the dimension of each sample is n, then the original sample set is an $n \times N$ matrix expressed as A. The dimension reduction model is an $r \times n$ matrix P, and the reduced sample set is an $r \times N$ matrix Y:

$$Y = PA = \begin{pmatrix} \vec{p}_1 \\ \vec{p}_2 \\ \dots \\ \vec{p}_r \end{pmatrix} \left(\vec{a}_1 \ \vec{a}_2 \ \dots \ \vec{a}_N \right) = \begin{pmatrix} \vec{p}_1\vec{a}_1 & \vec{p}_1\vec{a}_2 & \dots & \vec{p}_1\vec{a}_N \\ \vec{p}_2\vec{a}_1 & \vec{p}_2\vec{a}_2 & \dots & \vec{p}_2\vec{a}_N \\ \dots & \dots & & \dots \\ \vec{p}_r\vec{a}_1 & \vec{p}_r\vec{a}_2 & \dots & \vec{p}_r\vec{a}_N \end{pmatrix} = \begin{pmatrix} \vec{y}_1 \\ \vec{y}_2 \\ \dots \\ \vec{y}_r \end{pmatrix} \tag{13}$$

The new coordinates need to meet two requirements, which are a) the variance of the projection of each sample on each axis should be as large as possible and b) the covariances between the projections of samples on any two different axes is zero.

The two requirements can be meted by diagonalizing the covariance matrix of Y, expressed as CV:

$$CV = \frac{1}{N} YY^T = \begin{pmatrix} \frac{1}{N}\sum_{i=1}^{N} y_{1i}^2 & \frac{1}{N}\sum_{i=1}^{N} y_{1i}y_{2i} & \dots & \frac{1}{N}\sum_{i=1}^{N} y_{1i}y_{Ni} \\ \frac{1}{N}\sum_{i=1}^{N} y_{2i}y_{1i} & \frac{1}{N}\sum_{i=1}^{N} y_{2i}^2 & \dots & \frac{1}{N}\sum_{i=1}^{N} y_{2i}y_{Ni} \\ \dots & \dots & \dots & \dots \\ \frac{1}{N}\sum_{i=1}^{N} y_{Ni}y_{1i} & \frac{1}{N}\sum_{i=1}^{N} y_{Ni}y_{2i} & \dots & \frac{1}{N}\sum_{i=1}^{N} y_{Ni}^2 \end{pmatrix} \tag{14}$$

Transform CV as:

$$CV = \frac{1}{m} YY^T = \frac{1}{m} PA(PA)^T = \frac{1}{m} PAA^T P^T = P(\frac{1}{m} AA^T)P^T \tag{15}$$

Equation (15) shows that diagonalizing the covariance matrix of A is equivalent to diagonalizing the CV, and P is the eigen matrix of the covariance matrix of A. After obtaining P, the r eigenvectors with the largest eigenvalues are retained as the dimension reduction model. The projections of the samples on the r orthonormal vectors are larger than projections on other vectors, so the r projections are the principal components.

PCA is based on the linear transformation, and does not involve probability theory, so PCA also fits for small sample cases. Dimension reduction can bring two benefits, which are a) reduced the amount of calculation when training the classifier and running the classifier online and b) the extracted components are the projections with the largest variances in the new coordinate system, which makes the differences between different types of samples more obvious and concise.

C. A sampling strategy to implement the hybrid method online

The samples used to train the models should be obtained by sampling the three-phase current residual in a fixed phase range in each electrical cycle to comprehensively evaluate the three-phase current residual. In the PMSM variable speed system, the current sampling frequency is fixed, so the dimensions of the current residual samples within a fixed range of electrical cycle at different current frequencies are not equal. However, the offline trained models have fixed dimensions. Therefore, it is necessary to design a sampling strategy to make the dimensions of the residual samples at different current frequencies equal, so that the machine learning models can adapt to the variable speed system.

For the purpose of avoiding the interference of current distortion on the sampling process, the electrical angle, expressed asθ_e, calculated by the rotor position feedback is introduced in sampling. When the phase of A-phase current is zero, the corresponding θ_e is π. Assuming that the sampling process starts from the moment when θ_e is π, and a sample with fixed dimension n is sampled within $1/T$ electrical cycle, then the specific electrical angles triggering the sampling are:

$$\theta_e = \pi + j(2\pi/(n-1)T), j = 0,1...n-1 \tag{16}$$

By configuring the T and n, the dimensions and sampling range of the samples can be flexibly configured.

IV. Simulation Studies

The simulation of the proposed hybrid method is performed in MATLAB/ SIMULINK. The responses of the Luenberger observer under different conditions are simulated first. The feedback gains are K_1=K_2=12000. The initial speed command and load are 1000 rpm and 2 N.m, and T1 open-circuit is injected at 0.5 s. From 0.2 s, the load rises to 5 N.m and the speed command increases to 1500 rpm between 0.3 s and 0.4 s. The simulation results of speed, A-phase current, A-phase estimated current and the current residual are shown in Fig. 9.

Fig. 9 shows that current residuals satisfy the two characteristics of diagnosis variables. When there are changes in the load and speed, the current feedbacks vary in a relatively uniform manner, so the responses of the observer are quick enough to track the feedbacks well. So that the current residual fluctuates within a small range around zero. When a fault occurs, the A-phase current suddenly decreases to zero, and the feedback gains are not large enough to eliminate the errors, thus the current residual deviates from zero immediately.

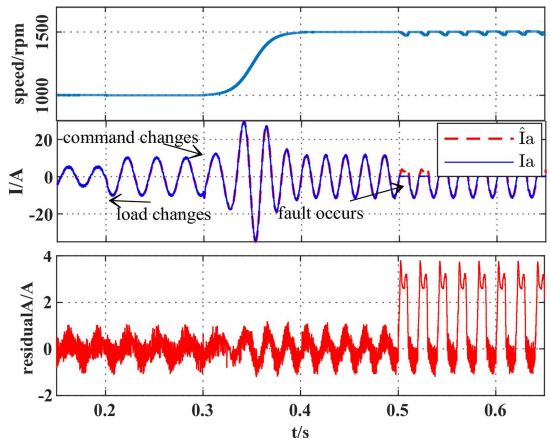

Fig. 9. Responses of the system and the observer under different conditions

Taking T1 open-circuit and T1T3 open-circuit as examples, the three-phase current residuals under these two conditions are shown in Figure 10:

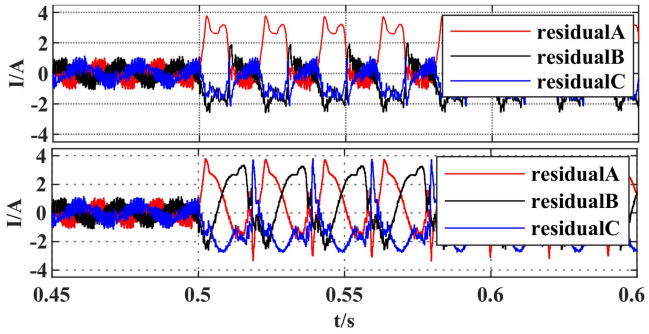

Fig. 10 Current residuals under T1 open-circuit and T1T3 open-circuit

Comparing the current residuals of T1 open-circuit and T1T3 open-circuit, these two faults have the same conduction path in the first quarter cycle when A-phase current is positive, that is, the A-phase leg of the inverter has no conduction path, and the B-phase and C-phase legs alternately conduct the positive and negative current. This leads to the similarity of the three-phase current residuals in polarity and change trend. If the diagnosis is carried out by comparing with a threshold value, the same diagnosis results would occur.

Then, using the designed sampling strategy, the samples with a fixed dimension of 100 are sampled in half an electrical cycle while the current frequency varies. The simulation results are shown as follows:

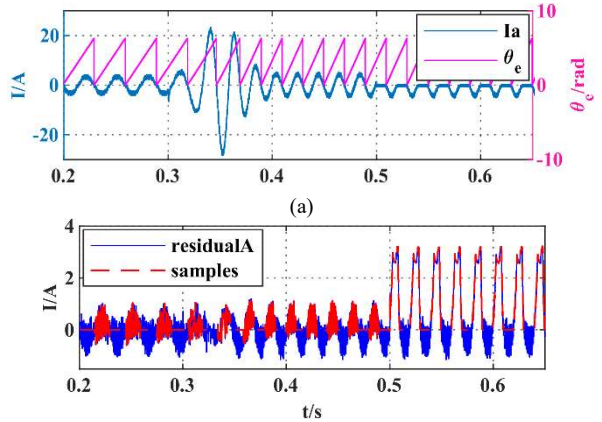

Fig. 11. (a) A-phase current and electrical angle under speed regulating (b) Current residual and residual samples under speed regulating

Fig. 11 shows the corresponding relationship between the A-phase current and the electrical angle, as well as the samples obtained by the sampling strategy during speed regulation. It can be seen that in a variable speed system, this sampling strategy can sample current residuals with a fixed dimension at different current frequencies.

As shown in Fig. 11. b, the current residual is expressed as a single value function in time domain. In this paper, PCA considers each residual sample as a vector in a high-dimensional space in which the number of coordinates, also can be called the dimensions, is equal to the number of sampling points. The directions and magnitudes of sample vectors are determined by the variation trend of three-phase residual along time. In other words, Different trends of residuals cause different vector distributions in the high-dimensional space. To highlight the different distributions of samples in different classes, PCA transfers the samples into a new coordinate system in the high-dimensional space according to the principle of maximizing variances. In this way, PCA extracts the principle distribution of the original samples in high-dimensional space and reduces sample dimension by storing the coordinates of the axes with the largest variances.

In this paper, each 30 residual samples are collected separately under the condition of no faults, T1 open-circuit, T1T3 open-circuit, and T1T4 open-circuit. Each sample consists of three-phase current residuals, and the residuals of each phase are sampled 100 times in half an electrical cycle. So the obtained original sample set is a 300×120 matrix, expressed as $X=[X_{health}, X_{T1}, X_{T1T3}, X_{T1T4}]$, in which X_{health}, X_{T1}, X_{T1T3}, and X_{T1T4} represent the 30 samples of no faults, T1 open fault, T1T3 open fault, and T1T4 open fault, respectively.

After obtaining X, the dimension of each sample in X is reduced to two by PCA. The obtained matrix after the reduction is called the training set which is a 2×120matrix, expressed as $XP=[XP_{health}, XP_{T1}, XP_{T1T3}, XP_{T1T4}]$. The distribution of XP is shown as:

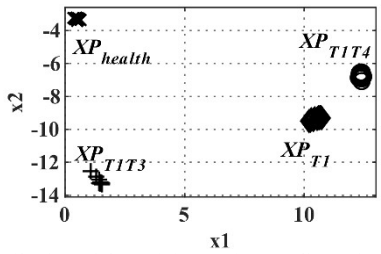

Fig. 12. The distribution of the training set in two-dimensional space

In Fig. 12, the two-dimensional space is the projection of the two axes with the largest variances in the high-dimensional space, and the 'x1' and 'x2' are the coordinates in these two axes. It can be seen that the four classes of samples in XP are linearly separable in two-dimensional space. If reducing the dimensions to one, the XP_{health} and XP_{T1T3} will overlap on the horizontal axis, and XP will become inseparable, so reducing the dimension of the original sample set to two is most appropriate. By reducing the dimensions, the distribution features of the three-phase current residuals in the high-dimensional space are retained, so that the differences between the four classes of samples are more obvious and

concise. Besides, the data amount of the original sample set is greatly reduced. These two benefits reduce the burden for subsequent training and online implementing.

Finally, a directed acyclic support vector machine (DAGSVM) is introduced to train the multi-classifier for fault diagnosis. DAGSVM can effectively reduce the calculation amount of multi-classifying process. Assume that there are K classes of samples. First, K (K-1)/2 binary classifiers need to be trained. Then, when making multi-classification decisions, DAGSVM only needs to call K-1 classifiers. For the four classes of samples, the six trained linear binary classifiers are shown in the Fig. 13:

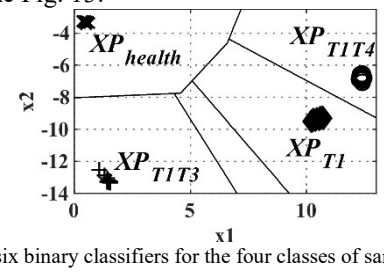

Fig. 13. The six binary classifiers for the four classes of samples

Test the multi-classifier with test samples. Taking a test sample of T1T3 open circuit as an example, the decision-making process of DAGSVM is shown as:

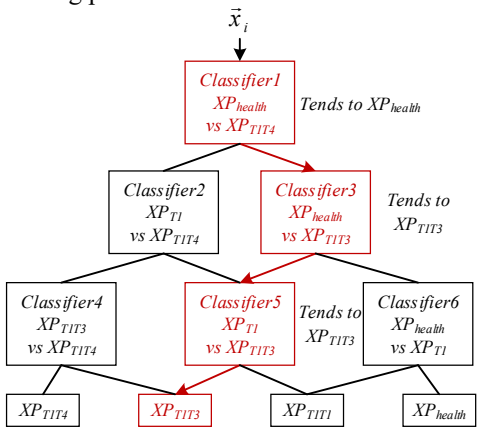

Fig. 14. The decision-making process of DAGSVM.

In Fig. 14, the red route represents the diagnosis route of the test sample. In each classifier, the diagnostic results tending to the left route are labelled as '-1' while the results tending to the right route are labelled as '1'. In the process of multi-classification, the test sample is evaluated by three binary classifiers for decision-making, and the final result is determined by the classifier conducting the last diagnosis and its corresponding diagnostic labels. The margins between the test sample and three classifiers are shown in Table II:

TABLE II
MARGINS BETWEEN THE TEST SAMPLE AND THREE DECISIVE CLASSIFIERS

Decisive classifiers	Margins between the sample and classifiers
*Classifier*1: XP_{health} vs XP_{T1T4}	0.6019
*Classifier*3: XP_{health} vs XP_{T1T3}	-1.0873
*Classifier*5: XP_{T1} vs XP_{T1T3}	-1.0428

It is known from Fig. 13 that XP_{health} and XP_{T1T3} are on the same side of *Classifier*1 in the two-dimensional space. So the classification result of the test sample on *Classifier*1 tends to XP_{health}, and in the subsequent evaluations of *Classifier*3 and *Classifier*5, the test sample is classified to XP_{T1T3}.

V. EXPERIMENTAL VERIFICATION

A PMSM drive based on TMS320F28335 is employed to verify the proposed online diagnosis method and is shown in Fig. 15.

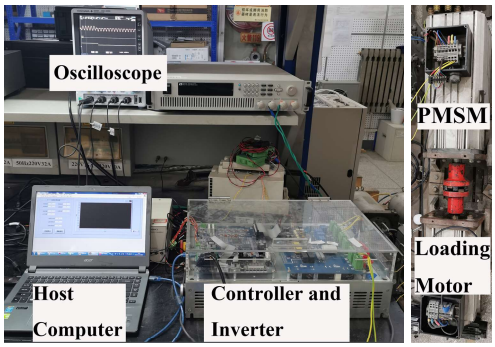

Fig. 15. The experimental platform

The ePWM module of TMS320F28335 contains a Trip-Zone (TZ) submodule which can flexibly configure the PWM signals as High, Low, or High-impedance, so TZ submodule is used in this paper to inject open circuit faults. The state variables inside the controller are transmitted to the oscilloscope for observation and acquisition through a D/A converter. A host computer sends commands to the controller via RS485. The parameters of PMSM used in this experiment are shown in Table III.

TABLE III
THE PARAMETERS OF THE EXPERIMENTAL PMSM

Parameter	Value
Number of pole pairs	4
Resistance of stator	0.306Ω
d axis inductance	2.4 mH
q axis inductance	2.4 mH
The flux of the rotor	0.281 Wb
DC voltage	60 V

Fig. 16 shows the dynamic responses of the Luenburger observer when the load varies between 3 N.m and 6 N.m. The load is increased from 3 N.m to 6 N.m in about 0.5 seconds. After 6 seconds, the load is reduced to the 3 N.m in a very short time. Regardless of whether the load gradually increases or drops abruptly, the current residual varies periodically within a constant range and is not affected by the changes of load.

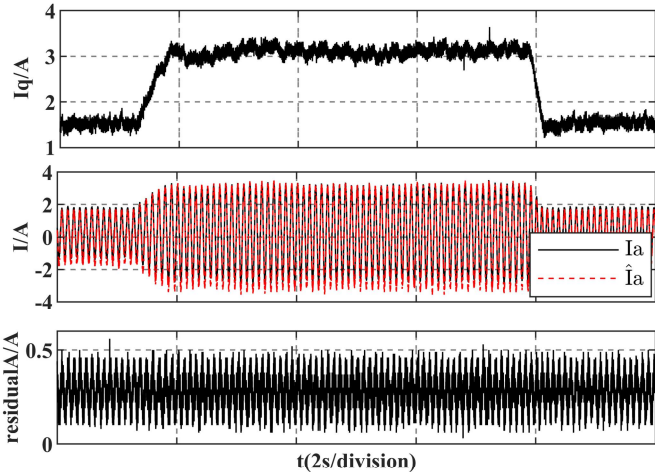

Fig. 16. The dynamic responses of Luenburger observer.

Figure 17 shows the three-phase current residual under T1 open-circuit, T1T3 open-circuit, and T1T4 open-circuit. In fault injection experiments, the three-phase current residual quickly deviate from zero and show different features according to different faults. As can be seen from Fig. 16 and Fig. 17, the current observation residuals meet the characteristics of being the diagnosis variables proposed in Section III.

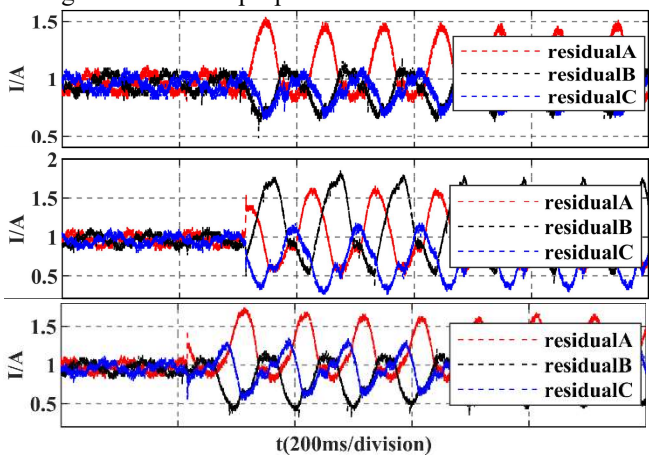

Fig. 17. The three-phase current residuals under T1 open-circuit, T1T3 open-circuit, and T1T4 open-circuit.

Fig. 18 shows the residual samples collected using the proposed sampling strategy under T1T3 open-circuit. Channel 1 of the oscilloscope is the A-phase current, and channels 2 to 4 are the current residuals of phase A, B, and C, respectively. It can be seen that the proposed strategy can sample current residuals with a fixed dimension in a fixed phase range of electrical cycle, to facilitate offline training and online implementation of machine learning models. After the original sample set is collected, the dimension reduction and training are performed offline. The resulting training set and six binary classifiers are shown in Fig. 19

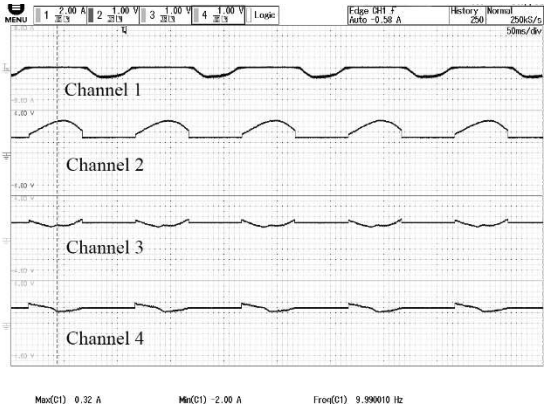

Fig. 18. Samples collected using the proposed strategy.

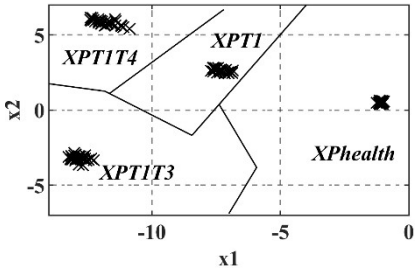

Fig. 19. The distribution of the training set and six trained binary classifiers.

T1 open-circuit is injected to test the performance of the proposed diagnosis method. The performance of the binary classifiers is tested first. Fig. 20 shows the evaluation result of the *Classifier* 6(XP_{health} *vs* XP_{T1}) before and after T1 open-circuit occurs. It can be seen that after the fault occurs, the calculation results are all smaller than -1 , which is, the diagnosis result is T1 open-circuit.

Then, test the performance of the DAGSVM. From Fig. 14, It is known that the samples of T1 open-circuit will be evaluated by the *Classifier* 1/2/5 sequentially to finally determine the diagnosis result. Fig. 21 shows the evaluation results of the *Classifiers* 1/2/5. Channel 1 of the oscilloscope is the A-phase current, and channels 2 to 4 are the evaluation results of the *Classifier* 1/2/5. It can be seen that the evaluation result of the *Classifier* 1 is negative, which leads the diagnosis result to T1T4 open-circuit, and then the evaluation results of the *Classifiers* 2/5 locate the diagnosis result to T1 open-circuit.

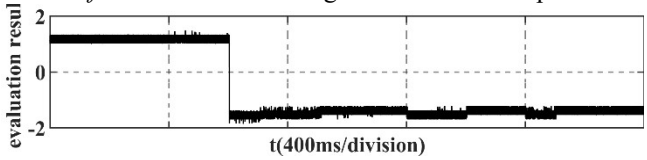

Fig. 20. The evaluation results of *Classifier* 5.

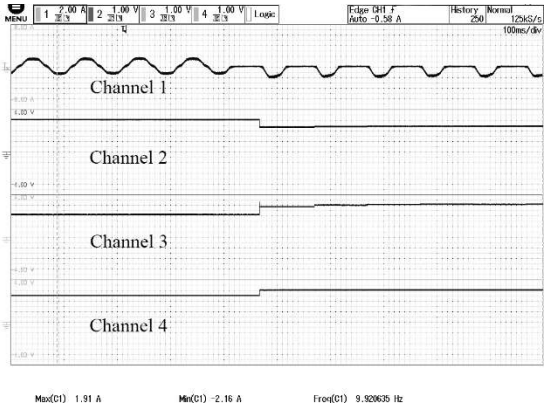

Fig. 21. The evaluation results of *Classifier* 1/2/5 when T1 open-circuit occurs.

The experimental result shown in Fig. 22 shows the shortest diagnosis time of the proposed method. In Fig. 22, the channel 1 is the A-phase current, and the channel 2 is the flag indicating the completion of the diagnosis. The High level represents that a fault has been located. As can be seen from Fig. 22, the diagnosis was completed in less than half an electrical cycle after the fault occurred in the experiment.

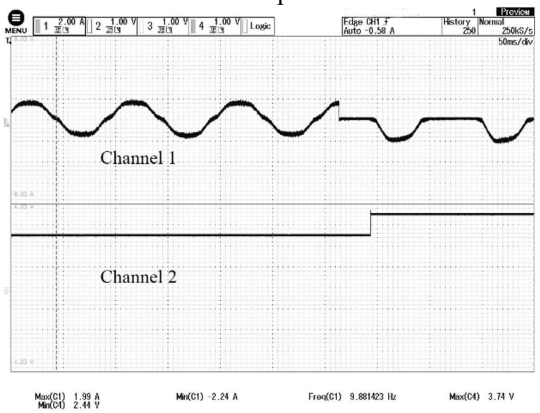

Fig. 22. The shortest diagnosis time in experiments.

Also, the computation of the proposed diagnosis scheme is tested and reported as below: In experiments, the TMS320F28335 works at 150 MHz. The switching period is 100 μs, and the PI controller, SVPWM and the observer account for maximum 25 μs. The process of dimension reduction requires 600 floating-point multiplications for each sample. Besides, the DAGSVM model is a series of binary linear equations, and each equation introduces 2 floating-point multiplications. The 600 floating-point multiplications are distributed over 6 switching cycles so that the total computation time at each cycle can be constrained below 50 μs. Therefore, the online implementation of the proposed diagnosis scheme does not cause influence on the motor control.

VI. Conclusion

PCA and SVM are introduced in this paper to comprehensively assess the three-phase current residuals obtained through a Luenburger observer. Besides, a sampling strategy is designed to implement this hybrid method online. The experiments verify that the proposed method can locate faults in less than half an electrical cycle and is able to classify the fault patterns whose responses show similarity. Online implementation and offline sampling are two major concerns for utilizing machine learning in electric drives. The proposed sampling strategy fulfills the requirements of online implementation, and improving the sampling process to reduce the data amount and the number of fault categories can be the next procedure of the research on machine learning based fault diagnosis.

References

[1] B. Lu and S. K. Sharma, "A Literature Review of IGBT Fault Diagnostic and Protection Methods for Power Inverters," *IEEE Transactions on Industry Applications*, vol. 45, no. 5, pp. 1770-1777, Sept.-oct. 2009.

[2] Chen Yong，Liu Zhilong， Chen Zhangyong. "Fast Diagnosis and Location Method for Open-Circuit Fault in Inverter Based on Current Vector Character Analysis," *Transactions of China Electrotechnical Society*，2018,33(04):883-891.

[3] C. Bae, D. Lee and T. H. Nguyen, "Detection and identification of multiple IGBT open-circuit faults in PWM inverters for AC machine drives," *IET Power Electronics*, vol. 12, no. 4, pp. 923-931, 10 4 2019.

[4] R. Peuget, S. Courtine and J. -. "Rognon. Fault detection and isolation on a PWM inverter by knowledge-based model, " *IEEE Transactions on Industry Applications*, vol. 34, no. 6, pp. 1318-1326, Nov.-Dec. 1998.

[5] A. M. S. Mendes and A. J. Marques Cardoso. "Voltage source inverter fault diagnosis in variable speed AC drives, by the average current Park's vector approach, " *IEEE International Electric Machines and Drives Conference. IEMDC'99. Proceedings (*, Seattle, WA, USA, 1999, pp. 704-706.

[6] A. J. Marques Cardoso and A. M. S. Mendes. "Semi-converter fault diagnosis in DC motor drives, by Park's vector approach, " *1996 Sixth International Conference on Power Electronics and Variable Speed Drives*, Nottingham, UK, 1996, pp. 93-98.

[7] X. Wu et al., "A Fast and Robust Diagnostic Method for Multiple Open-Circuit Faults of Voltage-Source Inverters Through Line Voltage Magnitudes Analysis," *IEEE Transactions on Power Electronics*, vol. 35, no. 5, pp. 5205-5220, May 2020.

[8] Z. Li et al., "A Fast Diagnosis Method for Both IGBT Faults and Current Sensor Faults in Grid-Tied Three-Phase Inverters With Two Current Sensors," *IEEE Transactions on Power Electronics*, vol. 35, no. 5, pp. 5267-5278, May 2020.

[9] Bae C J , Lee S M , Lee D C . "Diagnosis of multiple IGBT open-circuit faults for three-phase PWM inverters," *Power Electronics & Motion Control Conference*. IEEE, 2016.

[10] Estima J O , Freire N M A , Cardoso A J M . Recent advances in fault diagnosis by Park's vector approach[C]. *Electrical Machines Design Control & Diagnosis*. IEEE, 2013.

[11] Gao Z , Cecati C , Ding S X . "A Survey of Fault Diagnosis and Fault-Tolerant Techniques—Part I: Fault Diagnosis With Model-Based and Signal-Based Approaches," *IEEE Transactions on Industrial Electronics*, 2015, 62(6):3757-3767.

[12] Jlassi I , Estima J O , Khil S K E , et al. "A Robust Observer-Based Method for IGBTs and Current Sensors Fault Diagnosis in Voltage-Source Inverters of PMSM Drives," *IEEE Transactions on Industry Applications*, 2017, 53(3):1-1.

[13] Jlassi I , Estima J O , Sejir K E K , et al. "Multiple Open-Circuit Faults Diagnosis in Back-to-Back Converters of PMSG Drives for Wind Turbine Systems," *IEEE Transactions on Power Electronics*, 2015, 30(5):2689-2702.

[14] An Q T , Sun L , Sun L Z . "Current Residual Vector-Based Open-Switch Fault Diagnosis of Inverters in PMSM Drive Systems," *IEEE Transactions on Power Electronics*, 2015, 30(5):2814-2827.

[15] C. Yang et al., "Voltage Difference Residual-Based Open-Circuit Fault Diagnosis Approach for Three-Level Converters in Electric Traction Systems," *IEEE Transactions on Power Electronics*, vol. 35, no. 3, pp. 3012-3028, March 2020.

[16] Jung S M , Park J S , Kim H W , et al. "An MRAS-Based Diagnosis of Open-Circuit Fault in PWM Voltage-Source Inverters for PM Synchronous Motor Drive Systems, " *IEEE Transactions on Power Electronics*, 2013, 28(5):2514-2526.

[17] Maamouri R , Trabelsi M , Boussak M , et al. "A Sliding Mode Observer for Inverter Open-Switch Fault Diagnostic in Sensorless Induction Motor Drive," *42nd Annual Conference of IEEE Industrial Electronics Society.* IEEE, 2016.

[18] H. Yan, Y. Xu, F. Cai, H. Zhang, W. Zhao and C. Gerada. "PWM-VSI Fault Diagnosis for a PMSM Drive Based on the Fuzzy Logic Approach, " *IEEE Transactions on Power Electronics*, vol. 34, no. 1, pp. 759-768, Jan. 2019.

[19] M. A. Masrur, Z. Chen and Y. Murphey. "Intelligent diagnosis of open and short circuit faults in electric drive inverters for real-time applications, " *IET Power Electronics*, vol. 3, no. 2, pp. 279-291, March 2010.

[20] Dong-Eok Kim and Dong-Choon Lee. "Fault diagnosis of three-phase PWM inverters using wavelet and SVM," *2008 IEEE International Symposium on Industrial Electronics*, Cambridge, 2008, pp. 329-334.

[21] Cai B , Zhao Y , Liu H , et al. "A Data-Driven Fault Diagnosis Methodology in Three-Phase Inverters for PMSM Drive Systems, " *IEEE Transactions on Power Electronics*, 2016, PP(99):1-1.

Zeliang Zhang was born in Shaanxi, China, in 1995. He received the B.S. and M.S. degree in electrical engineering from Northwestern Polytechnical University (NPU), Xi'an, China, in 2017 and 2020. His research interests include motor control and fault diagnosis for electric drives.

Guangzhao Luo (Senior Member, IEEE) received the M.S. and Ph.D. degrees in electrical engineering from the Northwestern Polytechnical University (NPU), Xi'an, China, in 1998 and 2003, respectively.

From 2003 to 2004, he was a Postdoctoral Research at the University of Federal Defense, Munich, Germany. He is currently a Professor with

NPU. He is the Vice Director of the Rare Earth Permanent Magnet (REPM) Electric Machine and Control Engineering Center, Shaanxi Province. His research interests include advance control theory of permanent magnet electrical machine, high performance control technology of permanent magnet synchronous motor for electric traction and electric vehicle, real-time simulation technology for electrical drive system, and intelligence control of new energy conversion. Dr. Luo received the Second Prize from the China National Defense Science and Technology Progress Award in 1995 and 2011.

Zhengbin Zhang was born in Gansu, China, in 1986. He received the M.S. degree in pattern recognition and intelligent system from Shengyang Aerospace University Sheng'yang, China, in 2011 and 2014. He is currently working at Lanzhou wanli Aviation Electromechanical CO.LTD. His research interests include motor control and pattern recognition.

Xuecheng Tao was born in Anhui, China, in1993. He received the B.S. and M.S. degree in electrical engineering from Inner Mongolia University of Technology (IMUT) and Northwestern Polytechnical University (NPU)，Inner Mongolia and Xi'an, China in 2017 and 2020. His research interests include motor control and controller reliability analysis.